# INDUCED DRAG COMPUTATION WITH WAKE MODEL SCHEMES FOR HIGHLY NON-PLANAR WING SYSTEMS

J. Hoefling
J. Schirra, A. Spohr, D. Schaefer
FH Aachen University of Applied Sciences
Flight Systems, Flight Guidance and Control
52064 Aachen, Germany

**Abstract**

The capabilities of induced drag prediction for highly non-planar wing configurations are analyzed using a vortex-lattice, a relaxed-wake vortex-lattice and a higher order panel method. Therefore Surface Pressure, Trefftz-Plane and Trailing Edge analysis are studied using planar crescent and elliptical shaped lifting surfaces, concluding that the two latter methods achieve the desired accuracy. In order to study the influences of drag-free and force-free wake model schemes on highly non-planar configurations, two biplane configurations are analyzed. Each method were found to have span efficiencies that agree well with lifting line theory, yet the relaxed-wake vortex-lattice and the higher order panel methods achieved more accurate results regarding induced drag prediction. For the same biplane configuration different downwash distributions and spanlaodings are found, depending on the utilized force-free or drag-free wake model scheme. These differences are associated with the wake sheet and rollup behavior inherited by the force-free wake model scheme and verified by comparison to higher order methods.

## NOMENCLATURE

| | |
|---|---|
| b | span, [m] |
| $C_D$ | drag coefficient, [-] |
| $C_L$ | lift coefficient, [-] |
| $C_l$ | section lift coefficient, [-] |
| c | chord, [m] |
| dA | differential area element, [-] |
| D | drag force, [N] |
| e | span efficiency, [-] |
| h/b | height to span ratio, [-] |
| M | Mach number, [-] |
| n | unit normal vector ($n_x$, $n_y$, $n_z$), [-] |
| $N_c$ | no. chordwise elements per surface [-] |
| $N_s$ | no. spanwise elements per surface [-] |
| V | velocity vector (u, v, w), [m/s] |
| S | wing area, [m²] |
| x | streamwise axis, referenced to the root |
| y | spanwise axis coordinate |
| α | angle of attack, [°] |
| $\Gamma$ | circulation [m²/s] |
| Λ | aspect ratio, [-] |
| η | relative spanwise coordinate, [-] |
| ρ | density, [kg/m³] |
| Φ | perturbation potential, [-] |
| Δt | timestep size, [s] |

Subscript

| | |
|---|---|
| cres | crescent |
| ellip | elliptical |
| i | induced |
| LE | leading edge |
| SP | Surface Pressure |
| TP | Trefftz-Plane |
| TR | trailing edge |
| ref | reference |
| r | root |
| t | coordinate of wingtip |
| ∞ | freestream |

## 1. INTRODUCTION

Increasing fuel supply demand and long term climate change mitigation requires that further sustainable efficiency enhancements be made for the commercial aviation industry. For these necessities, induced drag reduction remains an attractive field of research, since this drag fraction occupies up to $40\%$ of total drag during cruise flight conditions for commercial transport aircraft [1]. In addition to conventional approaches like wing tip extensions rather unconventional approaches focused on highly non-planar wing configurations have regained attention in recent years. The key strategic goal of this study is to determine how accurately common numerical methods based on linear potential flow theory predict induced drag generation of highly non-planar configurations. Traditional vortex-lattice and panel methods model the trailing wake as drag-free flat vorticity sheet aligned with the freestream, which is leaving the wing trailing edge. Although the wake model scheme differs from the physical wake, accurate induced drag prediction for planar wings is possible using Trefftz-Plane integration. Nevertheless this method is strongly dependent on an accurate wake shape determination, which may prove difficult for multiple lifting surfaces. As such, trailing edge analysis, which is more independent of the farfield wake shape than Trefftz-Plane analysis, can thus be regarded as an alternative method for induced drag evaluation.

The applicability of a drag-free wake is no longer adequate for more sophisticated induced drag prediction, especially in the context of highly non-planar wing configurations like the biplane. Here, the vertical distance between the two wings generates a high degree of non-planar wake character. The applied force-free wake representation is aligned with the local flowfield and can capture significant non-linear effects due to wake rollup behavior. These effects are a consequence of the non-planar wake shape, which does induce forces on the wing itself and leads to interactions between the different lifting surfaces. In fact

Smith [2] used a hybrid wake-relaxation method to show that these high order effects should already be considered when making high accuracy drag prediction for planar wings, because some planar wings produce a non-planar wake shape. Introducing a non-planar closed wing system, induced lift becomes a unique non-linear influence of this arrangement, creating a not necessarily lift-free wake shed and conflicting with the drag-free wake model. The connection between induced drag and lift is therefore a critical issue, whose effects on the local flowfield are too significant to disregard.

Surface Pressure, Trefftz-Plane and Trailing Edge Analysis are especially suitable for numerical applications distinguished by low computational effort [3], when compared with high-fidelity methods and therefore indispensable for conceptual wing design. The objective of the present study is to examine the afore stated potential methods and consider any problems encountered with computational induced drag predication as they are applied on highly non-planar lifting surfaces.

## 1.1. Theory of Potential Methods

Prandtl´s classical lifting line theory, developed in the late 1920s reasons that a bound vortex in a flow will experience a lift force according to the Kutta-Joukowski theorem ( [1], [4]). Introducing a trailing vortex system at both end of the bound vortex the Helmholtz theorem became satisfied. By combining these theorems with Munks Stagger Theorem, which states that only the normal downwash of the trailing vortex system matters for drag purposes, a method for induced drag prediction was developed. The method derives that minimum induced drag is achieved by a uniform downwash distribution along the lifting line. Such a downwash is generated by an elliptical spanloading ( [5], [1]). The method was extended to a lifting surface method by Weissinger [5], who was implementing control points to satisfy the flow tangency condition. With these points it is possible to determine the bound circulation strength of the wake shed. This development led to the currently known vortex lattice and panel methods, which are using potential vortices, sources and sinks, distributed along the lifting surface.

The elliptical spanloading, which produces minimum induced drag, is not unique to a certain wing planform but can be applied to every planar wing due to changes in geometrical or aerodynamical twist distribution.

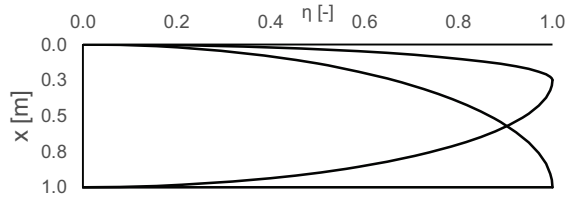


FIGURE 1: Crescent and elliptical planform

The family of wings studied in this paper consists of planforms with elliptical chord length distributions which are defined by the wing tip coordinate $x_t$ . The two analyzed planform shapes are the elliptical wing with a straight quarter chord line at $x_t = 0.25$ and the crescent shaped wing whose leading edge shows a higher eccentricity and posses a straight trailing edge at $x_t = 1.0$.

**Induced Drag Calculation**

Induced drag created by a finite wing is equal to the kinetic energy which is constantly added to the trailing wake system per distance traveled through the flowfield. Minimum induced drag is achieved for a uniform downwash distribution and elliptical circulation distribution [1]:

$$C_{Di} = \frac{2}{U_\infty S_{ref}} \int_{-b/2}^{b/2} \Gamma(y)\alpha_i(y)dy \quad (1)$$

Various approaches exist for inviscid and incompressible flow which provides acceptable accuracy as long as boundary layer effects, especially flow separation, are not dominant.

**Surface Pressure integration** is largely connected with the wing planform shape and the resulting pressure distribution. It is well-known that canceling the pressure gradients of the forward- and aftwards-facing wing surfaces results in pressure peaks which cannot be resolved properly and therefore are exposed to numerical errors [6]. Consequently, the precision of induced drag calculation is highly dependent on the quality of panel discretization, especially close to the leading edge and affected by angle of attack variations [7].

For **Trefftz-Plane integration** a finite wing is placed in a control volume which is extended to infinity. The induced drag can then be calculated by integration of pressure and momentum over the volume. The wake sheet far downstream is characterized by the velocity components $v$ and $w$ of the roll-up behavior and thus the velocity component $u$ in streamwise direction can be neglected [7]. With mass conservation stated the volume integral is reduced to a contour integral. In most application-oriented methods the integral is applied $18 - 36$ semi-spans downstream, along the intersection of the wake sheet with the control-volume rear face [6]:

$$D_i = {}^{\rho}/_{2} \iint (w^2 + v^2 - u^2)\, dA \quad (2)$$

The numerical approach to solve the contour integral is to place pairs of surveypoints in spanwise direction along the wake sheet in very small distances above and under the wake onto the Trefftz-Plane. Using these surveypoints the wake properties necessary for the integration can be determined, calculating the jump in potential across the wake [7]. Hence, the induced drag is related to the Gauss' theorem, the product of the integration of the potential jumps and the normal wash velocity through the wake defines induced drag:

$$D_i = {}^{\rho}/_{2} \iint (\Phi_{upper} - \Phi_{lower}) \frac{w_{i,TP}}{U_\infty}\, dy \quad (3)$$

Another method for induced drag evaluation is called **trailing edge analysis**, which is built on the consideration that all the vorticity created by the finite wing system is shifted into the trailing vortex [3]. This approach makes the wing trailing edge the origin where the wake-induced downward velocity $w$ is no longer prevented by the presence of the wing no perturbation constraint. Induced drag can therefore be evaluated by integrating the cross product of the lumped bound vorticity and the velocity

along the trailing edge induced by the wake [5]. Prior studies carried out by Bramesfeld [5] suggest that this approach is much less affected by detailed changes in the actual wake shape and already delivers precise results at a low discretization level.

### 1.1.1. Wake Modeling

The planar crescent shaped wing $(x_t = 1.0)$ is the most important case to validate the accuracy of the used methods because the wake trace resulting from the straight trailing edge is planar under all angles of attack [7]. This characteristic sets it apart from the classical elliptical wing $(x_t = 0.25)$, which creates an elliptical wake trace onto the Trefftz-Plane due to a certain angle of attack. The elliptical planform implies that a planar wing can indeed induce a non-planar wake and that the two analyzed wings with elliptical chord distribution are generating different wake shapes under angle of attack variation. When a drag-free wake model is used, the wake cannot generate any $u$-perturbations in Equation (2). This is because the wake model is aligned with the freestream and therefore the wake vorticity is perpendicular with the Trefftz-Plane. Nonetheless, drag-free wake model results can be considered accurate because the resulting error is in the magnitude of only $1\% - 2\%$ for planar wings and the significantly smaller computation effort justifies the usage compared to higher order methods [7].

However, for high accuracy induced drag calculation, including non-linear effects of planar wings and especially of highly non-planar wings systems like biplanes and closed -wings the differences in wake shape can no longer be neglected. For this reason a wake model scheme is to be used, modeling a “true” wake. Such a wake has to be force-free and aligned with the local flowfield behind a finite wing system. The two most commonly used methods are spatial-relaxation and time-stepping methods, while the latter requires less wake computing steps for the same flow-field size [5]. When a force-free wake model is applied $u$-perturbation is produced in the Trefftz-Plane because the wake is deflected with the local flowfield and no longer perpendicular to the Trefftz-plane [8].

Regardless of what force-free wake model scheme is used the choice of induced drag evaluation is either Trefftz-Plane or trailing edge analysis. Smith and Kroo [2] showed how sensitive Trefftz-Plane analysis is in respect to even small details in wake shape. In comparison, the wake shape quality – located far behind the wing in the Trefftz-Plane – does not have a significant impact on the trailing edge analysis [3]. Thereby using trailing edge analysis, additional endeavors to increase the wake shape resolution can be avoided.

### 1.2. Software used

**AVL** employs an extended vortex lattice method for the calculation of lifting surfaces using horseshoe vortices and a finite core option for the wake. For the panel discretization a uniform, sine and cosine distribution can be applied. Induced drag calculation can be carried out using both, Surface Pressure and Trefftz-Plane integration.

**Panair (A502)** is a high order panel method, applying a quadratic distribution of doublets and a linear distribution of sources over each panel with doublet and source matching at each panel edge [4]. Up to four different cases can be calculated at a time, supporting convergence studies of certain geometries. A half-cosine distribution was used for the spanwise panel discretization, concentrating more panels close to the wing tip in order to cover flow changes in this area. For induced drag calculation Surface Pressure and Trefftz-Plane integration are applicable.

**FreeWake** works with a number of distributed vorticity elements, which are used to model the particular wing. Each of these elements consists of a vortex filament at the leading- and trailing edge and an additional vortex sheet placed inbetween to ensure circulation continuity. Regarding the vortex sheet an individual selection of lifting lines in spanwise direction per element is possible, while the chordwise number is chosen for the whole wing. To capture second-order effects induced by the wake roll-up behavior a time marching force-free wake relaxation method is used, calculating the induced drag with a trailing edge analysis. In addition a Trefftz-Plane and Eppler analysis is carried out using a drag-free wake model [3].

## 2. DEFINITIONS AND CONVENTIONS

In order to standardize the analysis all cases were carried out with a fixed Mach number of $Ma = 0.2$. During the analysis it has been borne in mind that for practical aerodynamic design a variety of effects must be considered, but here the influence of a small Mach number on induced drag will be neglected. Within potential theory only induced vortex drag is present [1]:

$$C_{Di} = \frac{C_{Di,Ellip.}}{e} = \frac{{C_L}^2}{\pi \Lambda e} \tag{4}$$

According to lifting line theory $C_{Di,Ellip.}$ is the minimum induced drag for a planar wake, resulting from an elliptical span loading. The span efficiency factor $e$ depends on the planform lift and is mainly influenced by the planform shape [1]:

$$e = \frac{{C_L}^2}{\pi \Lambda C_{Di}} \tag{5}$$

Therefore the span efficiency is an essential way to compare the aerodynamic performance of different wing configurations. The theoretical value of an optimal planar wing is $e = 1$, for an optimal biplane $e = 1.36$ and a closed wing system like a Box-Wing configuration holds a value of $e = 1.46$. Constraining $b$ and $\Lambda$ as well as the angle of attack $\alpha$ is sufficient to create unique planform families for this study, staying within the constraints of isotropic scaling. The planform parameters of all two planar cases are shown in Table 1. No geometrical or aerodynamical twist was applied. The panel method was carried out using a NACA 0012 airfoil. The wing tips of the crescent and elliptical planform were cut off at a span-fraction of $\eta = 0.9995$ of the original half span to ensure that all cases were calculated with a finite wing tip [6]. All studies were carried out under an angle of attack of $\alpha = 4°$. Here, constraining the angle of attack instead of the lift coefficient is more reasonable for this study since the

purpose is to find out about the precision of induced drag prediction and to compare the found lift coefficients. Under these constraints the expected lift coefficient for a planar wing featured as flat sheet is about $C_L \cong 0.32$ and with airfoil about $C_L \cong 0.34$ [3].

| b/2 [m] | $S_{ref}$ [m²] | Λ [-] | $C_t$ [-] | $c_{ref}$ [m] |
|---|---|---|---|---|
| IDEAL CRESECENT WING | | | | |
| 2.745 | 4.318 | 7.0000 | 0.000 | 0.7854 |
| *CLIPPED CRESCENT WING* | | | | |
| 2.7453 | 4.318 | 6.9818 | ≈ 0.051 | 0.7854 |
| *IDEAL ELLIPTICAL WING* | | | | |
| 0.0000 | 0.000 | 7.0000 | 0.000 | 0.7854 |
| *CLIPPED ELLIPTICAL WING* | | | | |
| 2.7453 | 4.318 | 6.9818 | ≈ 0.051 | 0.7854 |

Table 1: Geometrical properties of analyzed planforms

## 3. VALIDATION

To confirm that the used methods are working for the proposed applications within defined tolerances to begin with, induced drag was computed for the planar elliptical and crescent shaped wing geometries. Therefore the induced drag and lift coefficients as well as the span efficiency were calculated for an increasing panel density. According to finite wing theory the span efficiency for both wings is $e = 1$ [1]. Based on the obtained results a statement concerning accuracy and reliability is possible. All methods are expected to calculate the two validation cases within a variation of less than $2\%$ compared to theoretical values.

### 3.1. Numerical sensitivity associated with paneling

In order to separate between the influences of spanwise or chordwise panel density variation, just one panel density was increased while the other remained constant.

#### 3.1.1. AVL

The convergence study was initialized first with $N_c = 50$ and secondly with $N_s = 20$, each time with a panel variation of $20 - 120$ in opposite direction. The majority of cases converged towards a span efficiency of $e = 1$ with a maximum error below $0.5\%$ despite the crescent wing, which was calculated with Surface Pressure integration and was showing a slightly higher error of max. $3.7\%$. Figure 2 show that the increasing panel density in chordwise direction just had minor or mostly no effect on the span efficiency- and induced drag results, independently if the results were found by Surface Pressure or Trefftz-Plane integration. Spanwise refinement had much stronger effect on the Surface Pressure integration, especially for the crescent wing with a span efficiency error decrease from $3.2\%$ to $1.2\%$ when $N_s$ was raised from $20$ to $120$.

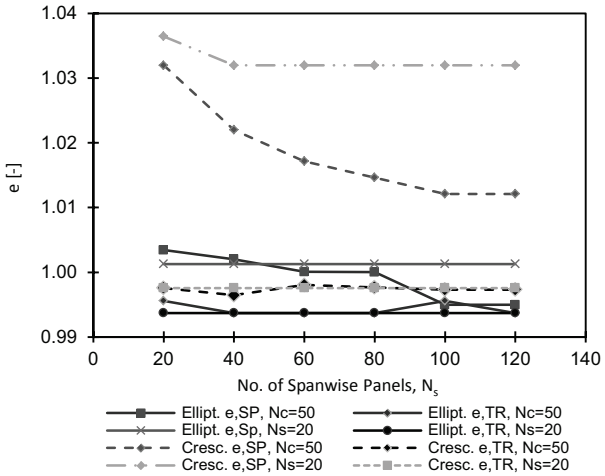


Figure 2: Span efficiencies found by AVL

#### 3.1.2. Panair

Considering problems with Surface Pressure integration the convergence study was started with a high panel resolution of $N_c = 50$ and growing number of panels $N_s$ in spanwise direction. Increasing the panel density from $N_s = 20$ to $N_s = 70$ the span efficiency error, using Surface Pressure integration decreased from $4.7\%$ to $1.7\%$ for the crescent wing, and from $2.7\%$ to $2\%$ for the elliptical wing. Further panel refinement strongly enhanced the necessary computational time and was therefore abandoned. Nevertheless the refinement showed good convergence behavior as can be seen in Figure 3, while the remaining error for both wings is about $2\%$ compared with the theoretical value. Additional analysis shows that the remaining error obtained with Surface Pressure integration was indeed strongly coupled to angle of attack variation. Comparing those results, the Trefftz-Plane analysis is barley affected by the same panel refinement in spanwise direction. The gained error in span efficiency is below $1\%$ for both wings. Respecting the results found by Trefftz-Plane integration the panel resolution in chordwise direction was cut in half, resulting in a hardly noticeable change in lift and drag coefficient, but in an appreciable reduction in computational effort.

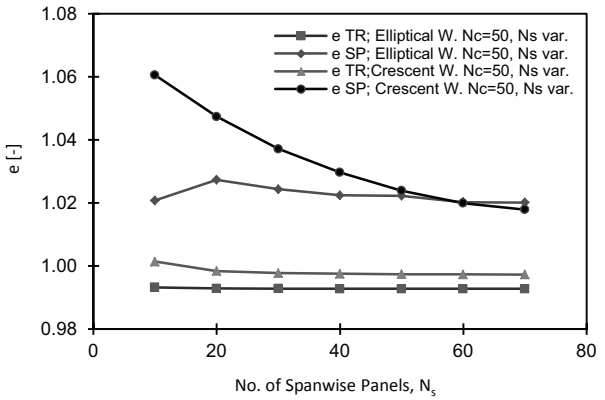


Figure 3: Span efficiencies obtained with Panair

The span efficiency results are confirmed by the early convergence behavior of the induced drag coefficient obtained by Trefftz-Plane analysis as they are compared

with the results found by Surface Pressure integration in Figure 3. The same applies in respect to the lift coefficient, while all results are slightly higher than the expected $C_L = 0.34$. There is also a general offset between the found results of the crescent and elliptical wing, while an equal panel density and the same method are used.

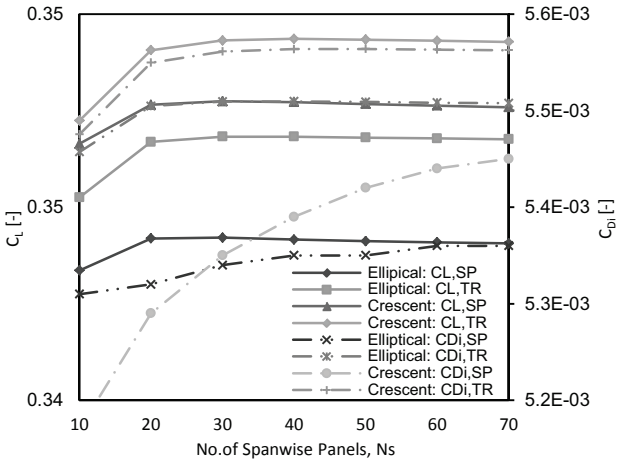


Figure 4: Effect on aerodynamic coefficients found by Panair for different panel densities

### 3.1.3. FreeWake

The error behavior for the crescent and elliptical wing is strongly related by the chosen width of each time step $\Delta t$ as well as the number of lifting lines in chordwise direction $N_c$. Nevertheless the span efficiency, induced drag and lift coefficient converge towards the theoretical value with increasing number of vorticity elements per panel as shown in Figure 5. Important is the fact that for a timestep of $\Delta t = 1$, both crescent and elliptical wing seem to converge towards a lower lift coefficient than the expected $C_L = 0.32$ and a higher span efficiency of up to $e = 1.12$. Increasing the number of vorticity elements per panel in spanwise direction from $1$ to $10$ brought a positive drop in span efficiency deviation from up to $21\%$ down to about $5\%$ for $t = 1$. After adjusting the timestep size to $\Delta t = 0.0025$ the span efficiency error is below $0.5\%$ for $N_c = 1$ and $N_c = 3$ and below $1\%$ for $N_c = 5$. All cases were showing excellent induced drag and lift coefficient convergence behavior.

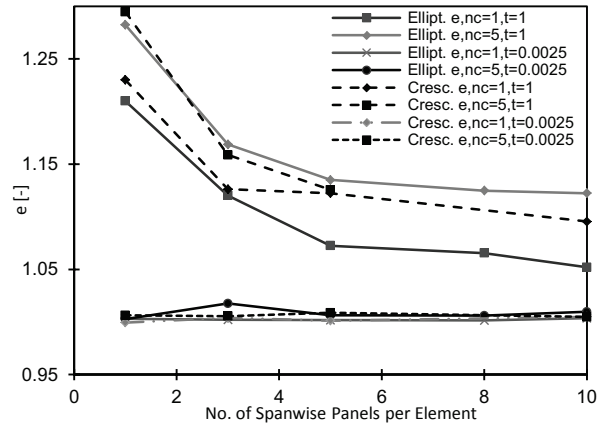


Figure 5: Span efficiencies predicted with FreeWake

## 3.2. Results and Discussion

In Table 2 the most accurate results of each method are listed, all of which were obtained with an individual panel density found by the respective convergence study. Special concern should be devoted to all results utilizing the crescent shaped wing. Recalling that the onto the Trefftz-Plane projected wake shape is straight under all angles of attack, what means that this wake behavior can be modeled with both wake model schemes. That leads to the conclusion that the results obtained for the crescent shaped wing should match linear theory results. The discrepancies left could be related to numerical issues and to the discrete nature of the singularities.

Despite that, the results gained by Surface Pressure integration are quite accurate when the cases comply with a sufficient panel resolution. Yet two additional interferences make this method unreliable. First is the existence of a planform dependent offset especially distinctive when the spanwise panel density is insufficient, which can only be diminished by accepting high computational effort. This problem is illustrated in Figure 4 and was first indicated by Smith and Kroo [6], experiencing the same phenomenon. Second is the strong correlation with angle of attack variation, restricting the usability of Surface Pressure integration even further than potential theory already does. For these two reasons, results obtained by Surface Pressure integration should be verified by a convergence study. Thus it can be concluded that the obtained results are not justifying the shouldered labor. In contrast Trefftz-Plane analysis delivers accurate results at a more reasonable panel discretization level, is less affected by planform shape variation, and is also far more accountable under angle of attack variations. Finally the results gained with the force-free wake model and trailing edge analysis is least effected by the used panel discretization level and works well with just one lifting line in chordwise and less than five in spanwise direction. Here the main attention lays on the right timestep size to require accurate results. When on the other hand an excessive panel density is used and an insufficient timestep size is chosen the necessary computational effort enhances rapidly compared to drag-free model with a similar discretization level.

In general it should be remembered that due to discretization limitations the circulation distribution is not uniform inheriting a finite vorticity at the wing tip and thus represents an almost elliptical span loading. When a linear panel distribution is used the resulting discretization error becomes especially significant at the wingtip. Here the induced velocity of the continuous circulation distribution remains finite, while the induced velocity of the discretized model deviates significantly. Whatever, a small error is likely to remain for all calculations using potential method.

## 3.3. Wake modeling effects

Concerning the differences between the crescent and elliptical wing all three methods generate the particular characteristic lift distribution. Figure 6 illustrates that the crescent wing holds a fuller section-lift distribution at the wing tip and smaller at the root. The ensuing span loading is therefore closer to a real elliptical distribution than the span loading produced by an elliptical planform with $x_{t=0.25}$.

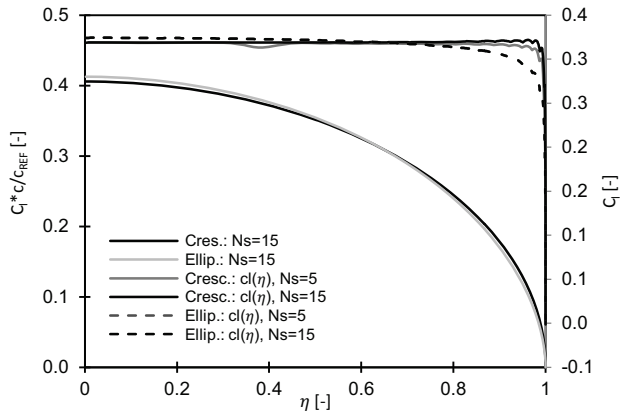


Figure 6: Spanloading and sectional lift coefficient distribution

Interpretations for these differences can be made taking a closer look at the downwash distribution in Figure 7. Here it is important to remember that the downwash distribution in FreeWake is plotted along the planform trailing edge, while the downwash evaluation in Panair carried out by Smith and Kroo [6], as well as the distribution obtained with AVL is generated in the Trefftz-Plane. The Trefftz-Plane results have the same properties, plotted in Figure 7. Both wings generate a constant downwash distribution going almost all the way up to the wing tip. Here the elliptical wing starts to create a decent amount of upwash. The downwash distribution of the crescent wing remains longer constant, before the downwash enhances. Induced upwash on the wing tip generates a certain amount of thrust and the crescent wing produces a higher drag and less lift, resulting from more pronounced downwash in Figure 7. The downwash distribution found by FreeWake is showing an increasing upwash behavior for both wings, especially noticeable for the crescent shaped wing. Similar characteristics were found by Schirra [9], using a higher order Euler code. These differences most likely find their origin in the wake rollup modeling. Hence, high panel resolution is necessary to model a preferable velocity distribution in this region.

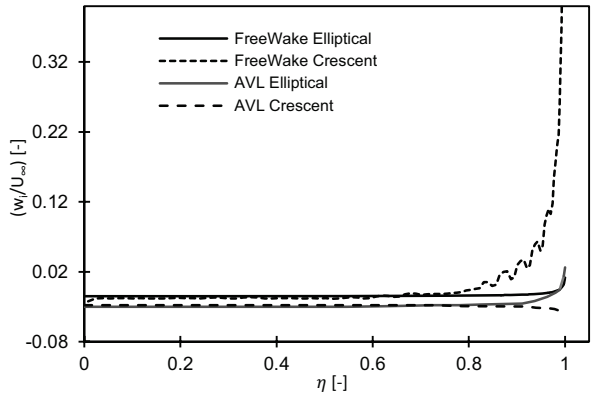


Figure 7: Downwash distributions in AVL and FreeWake

| | | $e_{SP}$ [-] | $e_{TP}$ [-] | $C_{L,SP}$ [-] | $C_{L,TP}$ [-] | $C_{Di,SP}$ [-] | $C_{Di,TP}$ [-] |
|---|---|---|---|---|---|---|---|
| Theory | | *1.0* | | *0.34* | | *5.257e-3* | |
| Panair | E. | *1.0208* | *0.9932* | *0.3434* | *0.3453* | *5.31e-3* | *5.46e-3* |
| | C. | *1.0179* | *1.0014* | *0.3476* | *0.3472* | *5.45e-3* | *5.48e-3* |
| AVL | E. | 1.0010 | 0.9959 | 0.3267 | 0.3242 | 4.85e-3 | 4.83e-3 |
| | C. | 1.0121 | 0.9986 | 0.3242 | 0.3242 | 4.70e-3 | 4.79e-3 |
| | | 1.0 | | 0.32 | | 4.6564e-3 | |
| FreeWake | E. | 1.0014 | | 0.3203 | | 4.66e-3 | |
| | C. | 0.9995 | | 0.3189 | | 4.62e-3 | |
| | | $e_{TR}$ [-] | | $C_{L,TR}$ [-] | | $C_{Di,TR}$ [-] | |

Table 2: Results of planar wing calculation

## 4. BIPLANE CONFIGURATION

The biplane configuration is the simplest highly non-planar wing configuration and is composed by the well-known crescent or elliptical planforms which were analyzed in the previous chapters (see Figure 8). The height to span ratio is based on Prandtl´s best wing system $h/b = 0.2$ [4]. Because the biplane is not a closed wing system, additional interaction between horizontal and vertical lifting surfaces are excluded, which is favorable in this early stage of analysis.

| b/2 [m] | η (b/2) [-] | $S_{ref}$ [m²] | Λ [-] | $c_r$ [m] | $c_t$ [m] | h/b [-] |
|---|---|---|---|---|---|---|
| 2.745 | 0.999 | 8.636 | 3,49 | 1.000 | 0.051 | 0.200 |

Table 3: Geometry of the biplane configuration

The biplane arrangement is also analyzed under an angle of attack of $\alpha = 4°$ and no angle of incidents is applied in between the two wings. Therefore the condition of minimum induced drag on each wing is violated as early as there are different induced angle of attack on the bottom and the top wing and theoretically mutual downwash interference. Schirra [9] analyzed the same biplane configuration using a higher order Euler solver, stating that when a NACA 0012 airfoil is applied the lift coefficient should be close to $C_L \cong 0.28$ for crescent planforms and slightly higher for elliptical planforms.

Figure 8: Crescent and elliptical biplane configurations

### 4.1. Numerical sensitivity associated with paneling of the biplane configurations

#### 4.1.1. AVL

Increasing the panel density in spanwise direction just rarely affects the span efficiency results. All found results have an error less than $1\%$ compared with theoretical values and hardly changed during the convergence study. For the highest panel density the crescent biplane configuration produces a span efficiency of $e = 1.3505$ and the elliptical biplane $e = 1.3476$.

Figure 9 shows that for an increasing panel density the particular lift coefficient remains almost constant and the changes of the induced lift coefficient are respectively to span efficiency and lift.

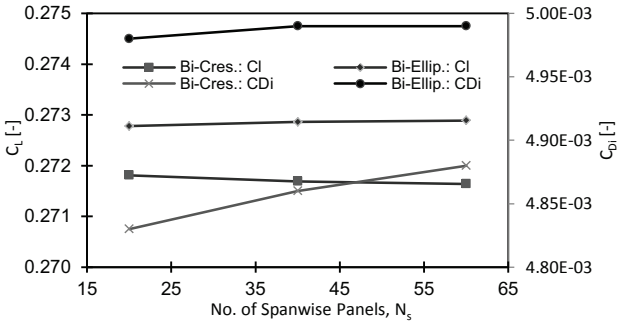


Figure 9: Lift and induced drag coefficient found by AVL for the biplane configurations

#### 4.1.2. Panair

The results obtained by Trefftz-Plane analysis are only marginally influenced by any panel resolution refinement. As with the planar wing configurations chordwise refinement shows no effect on the span efficiency, but even spanwise changes hardly make a difference. The span efficiency of the elliptical biplane is about $e = 1.345$ with an error of about $1\%$ and for the crescent biplane about $e = 1.355$ with an error of less than $1\%$. The lift coefficient shown in Figure 10 marginally decrease for a higher panel density in spanwise direction. Extending the convergence study further is not possible because the maximum number of panels is reached for two wings with $N_c = 5$ and $N_s = 70$.

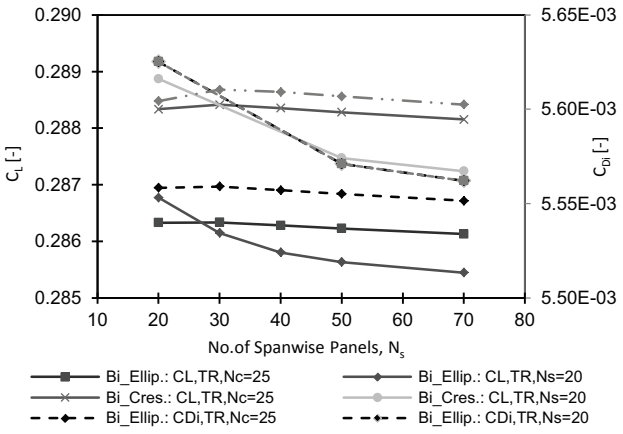


Figure 10: Lift and induced drag coefficients obtained by Panair for the biplane configurations

#### 4.1.3. FreeWake

The experience from chapter 3.1.3 shows that an inappropriate large time step size $\Delta t$ coupled with poor spanwise panel resolution lead to higher discrepancies compared with theoretical values. For the biplane case, an increased number of spanwise lifting lines lead nevertheless to convergence behavior, yet not necessarily towards reasonable values.

Figure 11 illustrates that the lift coefficient processes towards a lower lift coefficient of about $C_L \cong 0.25$ when the number of lifting lines in spanwise direction is increased. While this is not the expected convergence behavior towards the values found by Schirra [9], the particular span efficiency error does converge towards theoretical values. That means that due to insufficient timestep size inaccurate lift and induced drag coefficients are obtained, while a reasonable span efficiency is achieved. Concerning the initial results the error in span efficiency is up to $20\%$ for $\Delta t = 1$, $N_c = 5$ and $N_s = 1$ and falls down to $6\%$ for $N_s = 10$. Leaving the timestep unchanged and increasing the number of chordwise lifting lines does not advance the convergence behavior.

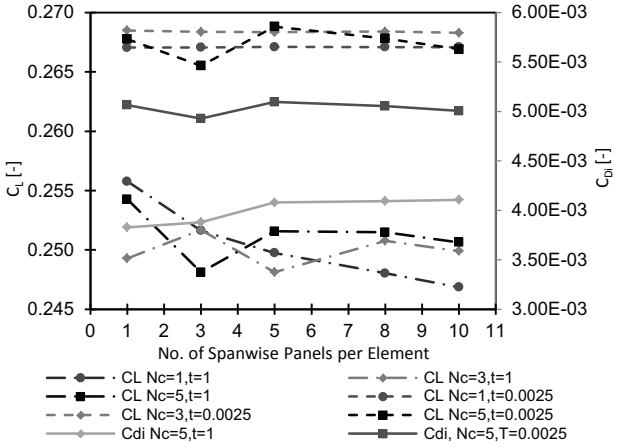


Figure 11: Lift and induced drag coefficient for the elliptical biplane configuration

The best convergence behavior and the most matching results are found by simultaneously adjusting the timestep size and increasing the panel density in spanwise direction, as can be seen in Figure 11. When the timestep size is reduced to smaller increments two phenomena can be discovered. First the initial calculation results at a very low panel density are better approximations than they were for the planar configurations. For the crescent biplane, inheriting a panel density of $N_s = N_s = 1$ the error in span efficiency dropped by the factor of $10$ when the timestep size is reduced by a factor of $20$. Secondly it causes a change in the convergence behavior, here shown in Figure 12 and Figure 13 for a high panel density of $N_c = 5$ and $N_s = 10$. When a rather high timestep size of $\Delta t = 0.5$ is used the lift coefficient of the elliptical biplane converges toward $C_L \cong 0.257$ and a span efficiency of $e = 1.3569$. On the other side the crescent biplane converges towards a much lower lift coefficient of $C_L \cong 0.22$ and a higher span efficiency of about $e = 1.41$. After changing the time step size to small increments of $t = 0.005$ the elliptical biplane converges towards lift coefficient of about $C_L \cong 0.269$ and the crescent biplane towards $C_L \cong 0.267$. Values in this magnitude were

expected, since no airfoil was applied. Under these circumstances the span efficiency of the elliptical biplane drops down to $e = 1.29$ and the span efficiency of the crescent biplane converges to $e = 1.356$. Here, the final induced drag coefficients lay also much closer together as for a timestep size of $t = 0.5$, plotted in Figure 12.

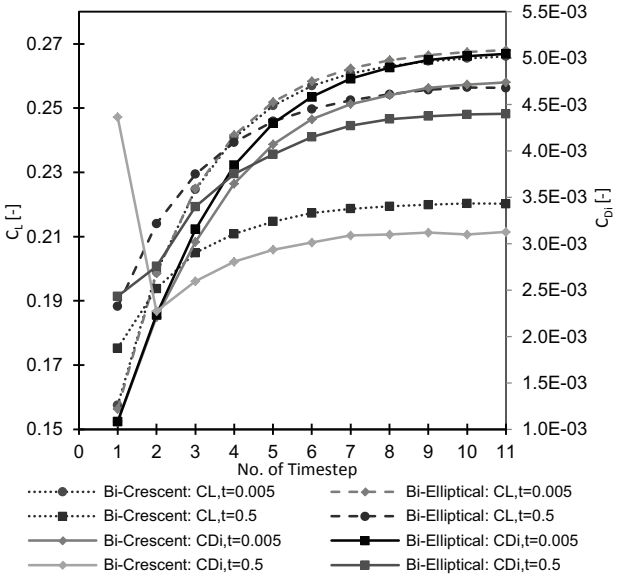


Figure 12: Lift and drag coefficient convergence behavior for time marching process and different timesteps

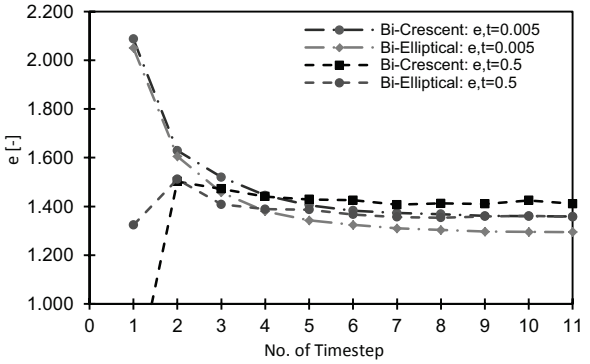


Figure 13: Span efficiency behavior for time marching process and different timesteps

### 4.1.4. Results and Discussions

In order to ensure comparability to a higher order method the results found by Schirra [9] are listed in Table 4. This study was carried out for the same biplane configurations, using a commercial Euler solver in ANSYS Fluent 14.5 with a cell-centered finite volume formulation for the Euler flow equations. Table 4 shows that Panair and AVL determine smaller span efficiencies for the elliptical biplane configuration than for the crescent configuration. The planform dependent relative variations in span efficiency are in the same magnitude as when compared with the reference values, with an relative error of less than $1\%$. Yet, the alterations of lift and induced drag coefficient are much stronger developed. The induced drag and lift prediction of Panair for the elliptical biplane is within a relative error of about $1\%$, but up to $6\%$ for the crescent shaped planform. The AVL performance is considerably poorer, expressed by a relative error of $9\%$ for the elliptical biplane and $8\%$ for the crescent.

Regarding the results obtained with FreeWake, the relative error in span efficiency for the crescent biplane is about $0.2\%$ compared to the reference value. Since no airfoil thickness is respected within FreeWake, a comparison of the lift- and induced drag coefficients is not applicable. Nonetheless, the crescent biplane results constitute the same characteristics than the reference values. But the elliptical biplane configuration seems to fall out the series, with a higher coefficient than the crescent biplane configuration and a span efficiency of $e = 1.2947$. Reasons for the large variations in span efficiency can only be suspected in association with the modeled wake rollup behavior and the timestep size of the wake relaxation method within FreeWake.

| | | e [-] | $C_L$ [-] | $C_{DI}$ [-] |
|---|---|---|---|---|
| Panair | E. | 1.3446 | 0.28610 | 5.55E-03 |
| | C. | 1.3513 | 0.28820 | 5.60E-03 |
| AVL | E. | 1.3476 | 0.27289 | 4.99E-03 |
| | C. | 1.3505 | 0.27164 | 4.88E-03 |
| FreeWake | E. | 1.2947 | 0.26691 | 5.00E-03 |
| | C. | 1.3542 | 0.26718 | 4.79E-03 |
| Higher Order [9] | E. | 1.342 | 0.2846 | 5.50E-03 |
| | C. | 1.352 | 0.2799 | 5.29E-03 |

Table 4: Results for the biplane configurations

### 4.2. Wake modeling effects

Figure 14 illustrates that there exists a distinct offset between the bottom and top wing´s sectional-lift coefficient distribution calculated by Panair and AVL. Close to the inboard section the bottom wing inherits an up to $15\%$ higher sectional-lift coefficient than the top wing. Regarding to the results found by FreeWake, this offset at the same location is much smaller. Here, the top wing possess a about $4\%$ bigger sectional-lift coefficient. The reason for the offset is suspected to be associated with a channel flow phenomenon between the two wings, whereby the higher coefficient of the top wing in FreeWake are most likely generated by wake rollup modeling. Regarding the individual sectional-lift coefficient distribution of each individual bottom or top wing, the distribution characteristics are very familiar with those of a planar wing in Figure 7: Downwash distributions in AVL and FreeWake. The crescent system shows a strong fluctuating growth close to the wing tip, while the elliptical biplane inherits a more rounded and decreasing distribution. The general offset of the section-lift coefficient induces a much higher spanloading on the bottom wing than on the top wing of each particular case.

When the crescent- and elliptical biplane configurations are compared among each other in Figure 16, the elliptical biplane configuration agrees much closer with a real elliptical shape, for both Panair and FreeWake. Yet, the

span loadings obtained with FreeWake are both slightly closer to the ideal elliptical distribution than compared to the Panair results. These discrepancies in Panair can be explained by the strong sectional-lift fluctuations at the outboard portion in Figure 14.

Even though the elliptical biplane configuration obtains a span loading closer to the ideal elliptical distribution, the span efficiency of $e = 1.3446$ is smaller when compared to $e = 1.3513$ of the crescent configuration. The reason for that is the action of the induced downwash distribution in relation to the circulation distribution in Equation (1). This effect is even more pronounced recalling the results found by FreeWake, with a span efficiency of $e = 1.29$ and a more ideal span loading for the elliptical biplane configuration. However, these strong discrepancies could be negatively enhanced by numerical issues within FreeWake, caused by the freestream velocity. Nonetheless the downwash- and sectional-lift coefficient distributions predicted by FreeWake are confirmed by the results found by Schirra [9].

## 5. CONCLUSION

Table 4 summarizes that the predicted span efficiencies are close to the theoretical values, despite the fact what wake model scheme is used. Greater differences become obvious concerning the accuracy of induced drag prediction. The vortex lattice method AVL deviates from comparative methods like the high order panel method Panair or the relaxed-wake vortex-lattice method FreeWake. The drag-free wake model scheme in Panair and AVL lacks in accurate downwash prediction, when compared to higher order results. But Panair provides highly accurate induced drag and lift results independent to a wide range of various planforms and boundary conditions. This states that the neglection of non-linear flow effects do not necessarily interfere with accurate induced drag prediction. Nevertheless, the force-free wake model scheme in FreeWake is able to predict accurate downwash patterns of highly non-planar lifting surfaces, which is suspected to make a higher impact on more complex wing arrangements and stabilizer-wing arrangements. Induced drag and lift can be predicted accurately, while a planform dependency concerning the span efficiency remains an unsolved issue.

In addition it is shown that the biplane configurations are generating stronger deviating span loadings in the outboard portion, when compared to the ideal elliptical shape. This does not lead to major performance deficits, caused by coupled relation of the particular downwash distribution and span loading on the induced drag. Concerning the necessary labor required to use these methods in an efficient design process, it can be stated the Panair is much more complex than AVL and FreeWake. This drawback can be compensated by a great amount of research done with Panair. In contrast FreeWake is already supplied with useful features to plot the wake shape and the velocity field.

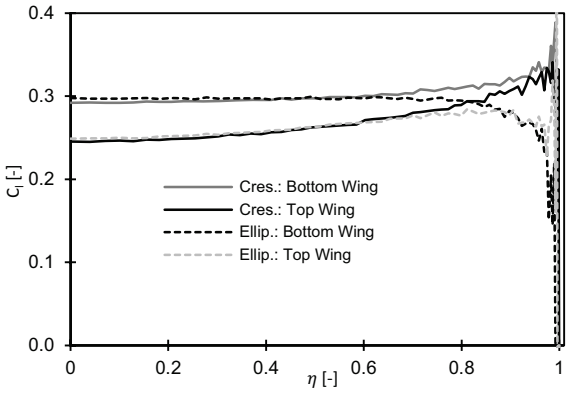


Figure 14: Sectional-lift distribution in Panair of the elliptical biplane configuration

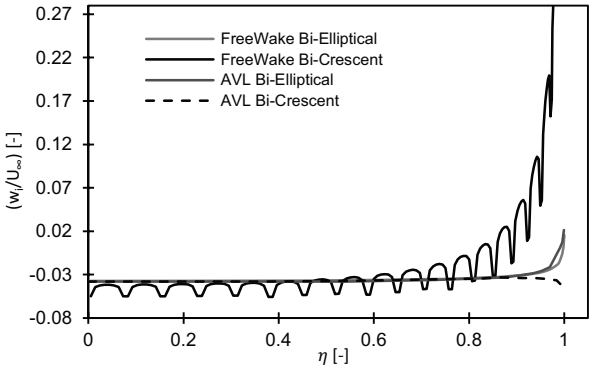


Figure 15: Downwash distributions in AVL and FreeWake

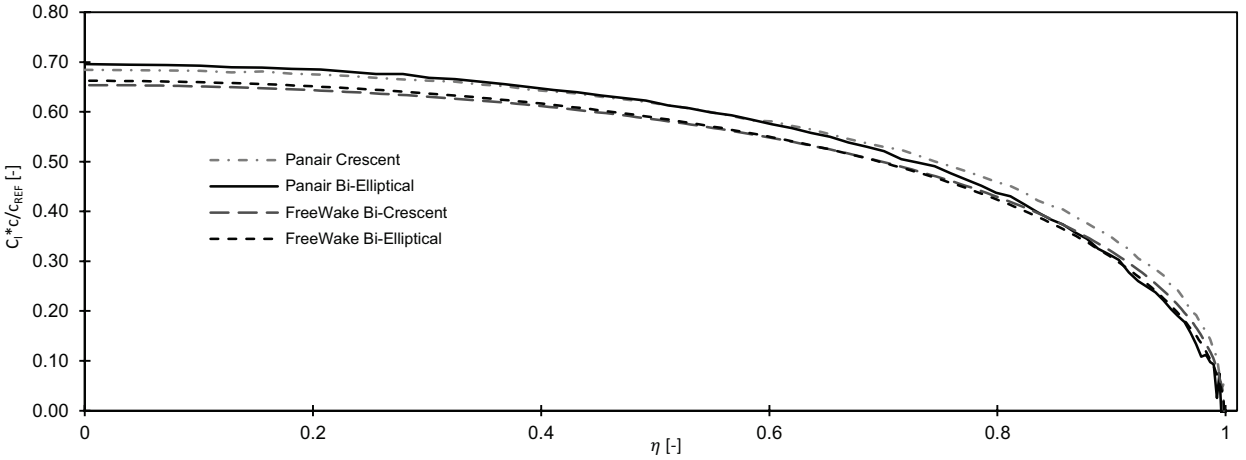


Figure 16: Total spanloadings found by Panair and FreeWake for the crescent and elliptical biplane configuration

## 6. References


1. **Anderson, J.** *Fundamentals if Aerodynamics.* New York,USA : McGraw-Hill, higher Educations, 2011. ISBN 978-007-128908-5.

2. **Smith, S. and Ilan, K.** *Induced Drag Computations on Wings with Accuratly Modeled Wakes.* s.l. : Journal of Aircraft, 1996. Vol. 34, No.2.

3. **Bramesfeld, G. and Maughmer, M.** *Relaxed-Wake Vortex-Lattice Method using distributed Vorticity Elements.* s.l. : Journal of Aircraft, 2008. Vol. 45, No. 2.

4. **Prandtl, L.** *Ergebnisse der Aerodynamischen Versuchsanstalt zu Göttingen, Lieferung 2.* Göttingen : s.n., 1923.

5. **Bramesfeld, G.** *A Higher Order Vortex-lattice method with a Force-Free Wake.* Pennsylvenia : Pennsylvenia State University, 2006.

6. **Smith, S. and Ilan, K.** *Computation of Induced Drag for Elliptical and Crescent-Shaped Wings.* Portland, OR : Journal of Aircraft, 1993. Vol. 30, No.4.

7. **Smith, S.** *A Computational and Experimental Study of Nonlinear Aspects of Induced Drag.* Moffett Field, California : NASA, Ames Research Center, 1996. NASA TN-3598.

8. **Hicken, J. and Zingg, D.** *Induced-Drag Minimization of Nonplanar Geometries Based on the Euler Equations.* British Columbia, Canada : AIAA Journal, 2010. Vol. 48, No.11.

9. **Schirra, J., Hoefling, J. and Spohr, A.** *Euler based Induced Drag Estimation for highly non-planar Lifting Systems during Conceptual Design.* Stuttgart : Deutscher Luft- und Raumfahrtkongress, 2013. 1284.

10. **Torenbeek, Egbert.** *Synthesis of Subsonic Airplane Design.* Dordrecht : Kluwer Academic Publishers, 1982. 90-247-2724-3.

11. **Kroo, I.** *Drag due to Lift: Concepts for Prediction and Reduction.* 2001.

12. **H. Schlichting, E Truckenbrodt.** *Aerodynamik des Flugzeugs Band 1 und 2.* s.l. : Springer-Verlag, 1968.

13. **Lam, F. and Maull, D. .** *Induced Drag of a Crescent Wing Planform.* s.l. : Journal of Aircraft, 1993. Vol. 30, No. 5.

14. **Letcher, J. Jr.** *Convergence of Lift and Drag Predictions by a Morino Panel Method (VSAERO).* s.l. : AIAA Journal, 1989. Vol. 27, No. 8.

15. **Dellann, M.** *Induced Drag of Wings with highly Swept and Tapered Wing Tips.* s.l. : AIAA, 1990. AIAA-90-3062-CP.